Multiwall Nanotubes, Multilayers, and Hybrid Nanostructures: New Frontiers for Technology and Raman Spectroscopy

Francesco Bonaccorso,[†] Ping-Heng Tan,[‡] and Andrea C. Ferrari[†,*]

[†]Cambridge Graphene Centre, University of Cambridge, 9 JJ Thomson Avenue, Cambridge CB3 0FA, United Kingdom and [‡]State Key Laboratory of Superlattices and Microstructures, Institute of Semiconductors, Chinese Academy of Science, Beijing 100083, China

ABSTRACT Technological progress is determined, to a great extent, by developments in material science. Breakthroughs can happen when a new type of material or new combinations of known materials with different dimensionality and functionality are created. Multilayered structures, being planar or concentric, are now emerging as major players at the forefront of research. Raman spectroscopy is a well-established characterization technique for carbon nanomaterials and is being developed for layered materials. In this issue of *ACS Nano*, Hirschmann *et al.* investigate triple-wall carbon nanotubes *via* resonant Raman spectroscopy, showing how a wealth of information can be derived about these complex structures. The next challenge is to tackle hybrid heterostructures, consisting of different planar or concentric materials, arranged "on demand" to achieve targeted properties.

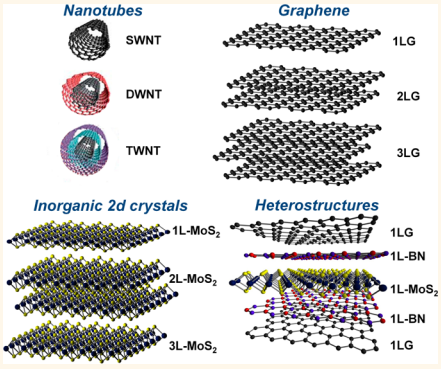

Graphene is the two-dimensional (2d) building block for graphitic materials of any other dimensionality. It can be wrapped into zero-dimensional (0d) fullerenes, rolled into one-dimensional (1d) nanotubes, or stacked into three-dimensional (3d) graphite.[1] The first evidence of nanotubes dates back to 1952,[2] with significant work performed in the 1970s.[3] This field came of age, with an exponential increase in publications, after multiwall nanotubes (MWNTs) were studied in 1991 with a high-resolution transmission electron microscope,[4] soon followed by single-wall nanotubes (SWNTs).[5] Depending on their diameter and chirality, SWNTs can be either metallic (m) or semiconducting (s). Their band gaps vary inversely with diameter.[6] One of the main goals of current nanotube research is to grow on-demand tubes of well-defined chirality. However, to date, most approaches result in heterogeneous samples, with only limited success in the selective growth of s-SWNT, m-SWNT, or SWNTs with narrow chirality distributions.[7] Selection can be achieved by dispersion and individualization in solution, followed by a sorting process[8] such as electrophoresis, chromatography, or density gradient ultracentrifugation, to cite a few. However, this typically requires the use of chemicals[9] that may be difficult to remove and may result in perturbations of the electronic and optical properties. Double-wall carbon nanotubes (DWNTs) are being tested in different areas,[10] including electronics (*e.g.*, field-effect transistors), photonics (*e.g.*, ultrafast optical switches), sensors (*e.g.*, mass sensors), and energy storage and generation (*e.g.*, supercapacitors and solar cells). The inner and outer tubes can be either metallic or semiconducting, with four different combinations (m@m, m@s, s@m, s@s) with distinct electrical, vibrational, and optical properties, not necessarily given by simple superpositions of those of the inner and outer layers.[11]

Optical techniques are ideal for probing nanotubes (see Figure 1): The measurements are nondestructive and can usually be carried out at room temperature, under ambient pressure, with minimal sample preparation. Variations in the surrounding dielectric environment due to solvents,

* Address correspondence to acf26@eng.cam.ac.uk.

Published online March 08, 2013
10.1021/nn400758r

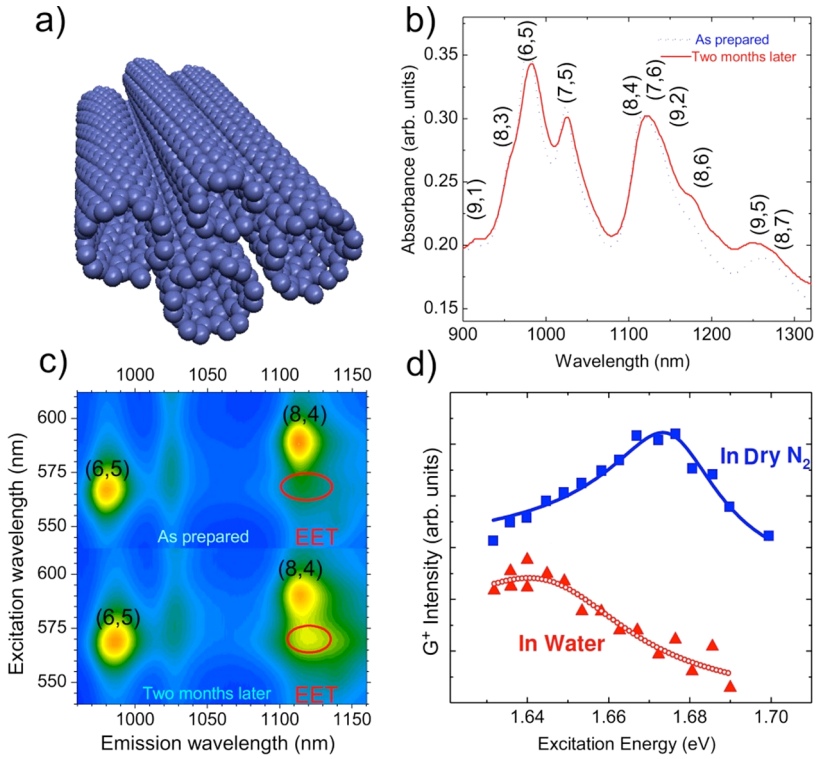

Figure 1. (a) SWNT bundle, (b) absorption spectra of SWNTs dispersed in water with sodium docecylbenzenesulfonate surfactant. Blue curve, as prepared sample, red curve after 2 months. (c) PLE map of as-prepared sample (top) and after 2 months (bottom), where red ellipses show the EET-induced features. (d) Raman intensity of the G^+ band as a function of the excitation energy for a single SWNT measured in dry N_2 in an enclosed chamber and immersed in water. Adapted from ref 13. Copyright 2007 American Chemical Society.

dispersants, or bundling (Figure 1a) cause the electronic properties of nanotubes to change. Such changes can be probed by optical absorption spectroscopy (OAS; Figure 1b), photoluminescence excitation (PLE) spectroscopy (Figure 1c), and Raman spectroscopy. As shown in Figure 1b,c, after incubation for 2 months for an as-prepared SWNT dispersion, the absorption and PL emission of a specific SWNT red shift because of aggregation in bundles. Bundling induces red shift and broadening of excitonic transitions.[12] The red shift is attributed to modifications of Coulomb interactions by the dielectric screening of adjacent tubes.[12] The optical transitions of SWNTs are also modulated by different dielectric environments (Figure 1d).[13] Bundling and dielectric effects can be detected in OAS and PLE. Exciton energy transfer (EET) from large gap tubes to smaller ones is efficient in bundles.[14] The EET signatures in PLE can identify whether the shift of PL and OAS is induced by the change of dielectric environment around a SWNT.[14] Raman spectroscopy is one of the most used characterization techniques in carbon science and technology, being the method of choice to probe disordered and amorphous carbons, fullerenes, nanotubes, graphene, graphite, diamonds, carbon chains, and polyconjugated molecules.[15] Resonant Raman spectroscopy can assign tube diameters through the radial breathing modes (RBMs)[16] and G peak position.[17] The resonant Raman profile is also sensitive to the environment; for example, Figure 1d shows that, when compared to measurements in dry N_2, the resonant Raman profile measured in water red shifts.

SWNTs, and the outer tube in MWNTs, are in direct contact with the environment, and their properties can be affected by it. In this issue of *ACS Nano*, Hirschmann *et al.*[18] perform resonant Raman spectroscopy on triple-wall nanotubes (TWNTs) prepared from high-temperature treatment of DWNTs encapsulating fullerenes. They show that the inner s-SWNTs are more affected by intertube interactions than m-SWNTs. The shifts and changes in line shapes of both RBMs and G peaks are used to quantify the effects of intertube interactions, as well as how outer concentric tubes affect the electronic and vibrational properties of inner tubes. Hurschmann *et al.* find that the smaller the tubes, the larger the difference of the environmental effects on m- and s-tubes, the latter being more affected by intertube interactions, especially for smaller diameters.[18]

Optical techniques are ideal for probing nanotubes.

Graphene Multilayers. Environment also plays a key role in planar

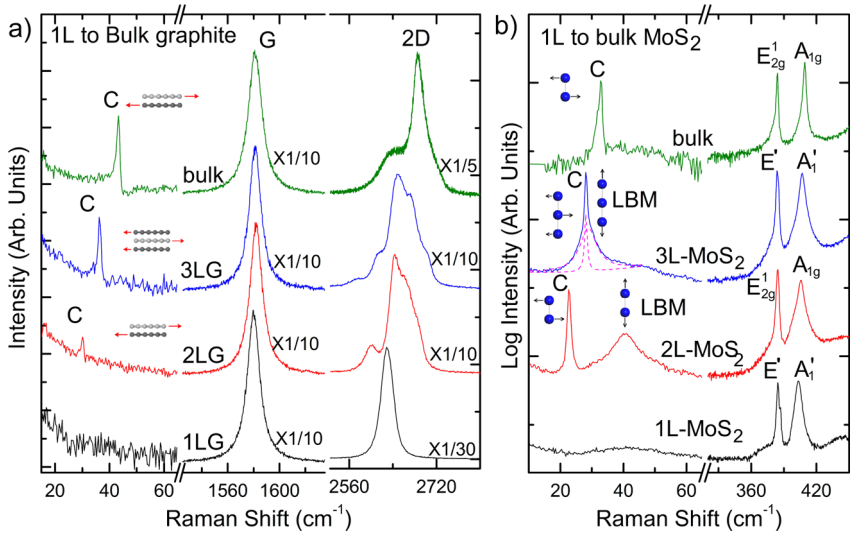

Figure 2. (a) Raman spectra of SLG (1LG), BLG (2LG), TLG (3LG), and bulk graphite measured at 633 nm. (b) Raman spectra of 1L-MoS_2, 2L-MoS_2, 3L-MoS_2, and bulk MoS_2 measured at 532 nm.

structures. For example, mobilities up to 10^7 cm^2 V^{-1} s^{-1} at 25 K were reported for decoupled single-layer graphene (SLG) on the surface of bulk graphite[19] and up to 10^6 cm^2 V^{-1} s^{-1} on current-annealed suspended SLGs,[20] while room temperature mobilities up to ~20 000 cm^2 V^{-1} s^{-1} were measured in SLGs on Si/SiO_2.[21] Mobilities in excess of 10^5 cm^2 V^{-1} s^{-1} can be achieved for SLGs encapsulated between exfoliated hexagonal boron nitride (h-BN) layers.[22]

The properties of multilayer graphene (*e.g.*, bilayer, BLG, and trilayer, TLG) vary with stacking order[23] and with relative twist.[24] In BLG, a transverse electric field can open a gap up to 250 meV,[25] whereas in TLG with ABA stacking, there is no gap.[26] On the other hand, ABC-TLG can have a tunable gap *via* the gate voltage, up to 120 meV.[27] Raman spectroscopy is ideal for characterizing graphene flakes.[28,29] The 2D peak changes in shape, width, and position with the number of layers (*N*), reflecting the changes in the band structure. The 2D peak is a single band in SLG, whereas it splits in four in BLG (Figure 2a).[30] Multilayers can have 2D peaks resembling that of SLG if the layers are decoupled, such as by a random twist.[24] The Raman spectra probe electron−phonon, magneto−phonon, and electron−electron interactions and change with the number and orientation of layers, electric or magnetic fields, strain, doping, disorder, quality, types of edges, and functional groups.[29]

Few-layer graphene flakes (FLGs) can also be characterized by the interlayer shear mode, derived from the low-energy E_{2g} mode in bulk graphite[31] (see Figure 2a), that is, the C peak that probes the interlayer coupling.[32] This peak scales from ~44 cm^{-1} in bulk graphite to ~31 cm^{-1} in BLG (see Figure 2a).[32] Its low energy also makes it a probe of near-Dirac point quasi-particles, giving a Fano line shape, due to resonance with electronic transitions. Layer breathing modes (LBMs) can also be observed in the Raman spectra of FLGs, *via* their resonant overtones in the range 80−300 cm^{-1}.[33] Because the fundamental LBM in bulk graphite is a silent B_{1g} mode at ~128 cm^{-1},[34] the observation of the first-order LBM is a challenge.

SLG cannot have C or LB modes, due to the lack of layer coupling. Upon rolling the sheet into a cylinder, the acoustic mode in which atoms move perpendicular to the plane will correspond to the RBM of the cylinder, with atoms vibrating along the radial direction.[35] Its position, Pos(RBM), is inversely related to the SWNT diameter,[16,36] *d*, as Pos(RBM) = $C_1/d + C_2$. A variety of C_1 and C_2 values were proposed for this relation.[15] For few-wall carbon nanotubes, such as DWNTs and TWNTs, the interwall distance is close to the layer distance in bulk graphite; thus, the wall coupling is expected to be weak. Indeed, in this issue of *ACS Nano*, Hirschmann *et al.*[18] show that the inner peapod-derived nanotubes in DWNTs and TWNTs have similar properties and, in both cases, the degree of isolation of these inner tubes depends on them being metallic or semiconducting. It should be noted that LBMs in FLGs are collective vibrations of all layers, while RBMs in DWNTs and TWNTs are due to specific walls.

Inorganic Multilayers. Raman spectroscopy also has potential for the characterization of layered materials (LMs) other than graphene. There are several LMs, studied since the 1960s,[37] which retain their stability down to monolayers and whose properties are complementary to those of graphene. Transition metal dichalcogenides (TMDs) and transition metal oxides (TMOs) have layered structures.[37] Atoms within each layer are held together by covalent bonds, while van der Waals interactions hold the layers together.[37] The pool of 2d crystals is

huge and covers a massive range of properties.[37] For example, $NiTe_2$ and VSe_2 are semimetals,[37] WS_2, WSe_2, MoS_2, $MoSe_2$, $MoTe_2$, TaS_2, $RhTe_2$, and $PdTe_2$ are semiconductors,[37] h-BN and HfS_2 are insulators, NbS_2, $NbSe_2$, $NbTe_2$, and $TaSe_2$ are superconductors,[37] while Bi_2Se_3 and Bi_2Te_3 are thermoelectrics[37] and could be topological insulators.[38] All of these can be exfoliated as is done for graphene.[39] LMs have been used as solid lubricants because of their tribological properties.[40] In addition, the mechanical properties of some 2d materials (*e.g.*, BN and MoS_2) make them attractive as fillers to reinforce plastics.[41] Thin LM films may be used for thermoelectric devices.[42] TMOs, in particular, MnO_2 sheets, are promising for supercapacitors and batteries.[43] They also have photoelectrochemical properties,[44] with photon-to-electron conversion efficiencies comparable to those of dye-sensitized solar cells, and are thus of interest for photovoltaics (PV).[45] Other uses, such as in light-emitting diodes,[46] ion exchangers,[47] and photocatalysts,[48] *etc.*, have already been demonstrated. Similar to graphite and graphene, the LM properties are a function of *N*. For example, bulk MoS_2 has an indirect band gap,[49] while a monolayer has a direct band gap[23] that could be exploited for optoelectronics.[50]

Raman spectroscopy also has potential for the characterization of layered materials other than graphene.

Raman scattering is also useful for the study of inorganic LMs, from bulk to monolayers.[51] For example, the Raman spectrum of bulk MoS_2 consists of two main peaks at ~382 and ~407 cm^{-1} (Figure 2b)[34] assigned to E^1_{2g} in-plane and A_{1g} out-of-plane modes, respectively.[34] The former red shifts, while the latter blue shifts with the number of layers (*N*; see Figure 2b).[52] Moreover, they have opposite trends when going from bulk MoS_2 to 1L-MoS_2, so that their difference can be used to monitor *N*.[52] However, the trends are not fully understood, and more work is needed to clarify the changes with *N*. Raman spectroscopy of C and LB modes is also a useful tool to probe these materials. These modes change with *N*, with different scaling for odd and even *N*.[51] With the increase of *N*, the frequency of the observed C mode of multilayer MoS_2 blue shifts, while that of LBMs red shifts, as shown in Figure 2b. The C and LB frequencies, $\omega(N)$, of a LM with *N* layers depend on *N* as follows: $\omega(N) = \omega(2)\sqrt{1 \pm \cos(N_0\pi/N)}$ ($N \geq 2N_0$, and N_0 is an integer: 1, 2, 3, 4...). This formula can be generally applied to any LM, allowing a diagnostic of their thickness.[51]

Heterostructures and Hybrids. LMs can be exploited for the realization of heterostructures. The combination of 2d crystals in 3d stacks offers huge opportunities in designing the functionalities of the resulting stacks.[53,54] One might combine conductive, insulating, superconducting, and magnetic 2d materials in one stack with atomic precision, fine-tuning the performance of the resulting material. Furthermore, the functionality of such stacks is "embedded" in the design of such heterostructures.[53] These heterostructures already play crucial roles in technology, with the development of semiconductor lasers[55] and high-mobility field-effect transistors (FETs).[56] Most importantly, the functionality of such heterostructures is not simply given by the combined properties of the individual layers. By carefully choosing and arranging the individual components, one could, in principle, tune the parameters, creating "materials on demand"[53] with properties tailored for targeted applications; for example, superstructures can be used for tunnel devices, such as diodes, FETs, and light-emitting devices, or for energy applications, such as PV cells. The first examples have already started to appear, such as vertical tunneling transistors[54] showing ON/OFF ratios of ~10^6. Graphene/quantum dot hybrids, with strong absorption,[57] have been investigated for photodetectors and image sensor arrays.[58]

The interactions between different layers inside heterostructures and hybrids are expected to be weak if van der Waals forces hold them together. In this case, the vibrations of heterostructures and hybrids will consist of those from the individual building blocks. Therefore, Raman spectroscopy is expected to be useful to probe the stoichiometry of heterostructures and hybrids. For example, the Raman peaks from graphene and $FeCl_3$ can be identified in $FeCl_3$-intercalated FLGs,[59] while at the same time probing the layer coupling, stability, charge transfer, strain, and orientation.[59] Surface-enhanced Raman scattering is observed in hybrids with metal dots,[60] while Raman spectroscopy can also be used to monitor/optimize growth conditions for heterostructures and hybrids.[61] Considering a 2L-BN/SLG/2L-BN structure on a substrate, one could observe Raman peaks from upper and lower 2L-BN as well as from the SLG. The coupling between BN and graphene would be reflected in modifications of the spectra with respect to isolated components.

OUTLOOK AND FUTURE CHALLENGES

Intrawall and intralayer optical modes of FLGs, SWNTs, and MWNTs mainly appear in the high-frequency region above 1000 cm^{-1}. The shear and layer (radial) breathing modes are usually located in the low-frequency region below 500 cm^{-1}. For LMs, such as transition metal dichalcogenides, the peak position of intrawall and intralayer optical modes is below 500 cm^{-1}, while shear and layer (radial) breathing modes are below 100 cm^{-1}, as shown in Figure 3.

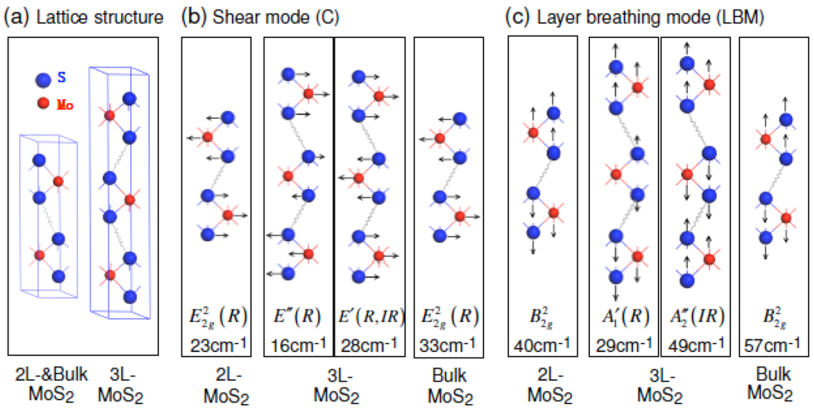

Figure 3. (a) Lattice structures of 2L-MoS_2 and bulk (left) and 3L-MoS_2 (right). (b) Shear modes and (c) LBMs in 2L-MoS_2, 3L-MoS_2, and bulk MoS_2. Adapted with permission from ref 51.

In multiwall tubular structures, each layer can produce a RBM, and, in principle, there also exists a set of collective wall shear and breathing modes, similar to the case of planar 2d crystals, as shown in Figure 3a with lattice structures and Figure 3b,c with the corresponding modes for FL-MoS_2. For FLGs, the observation of the first-order LBMs is still a challenge because of low frequency and Raman inactivity. In tubular structures, besides the wall breathing modes, there is also a set of cylindrical shear modes (telescope and rotary modes)[35] similar to the case of the shear modes in planar 2d crystals, as shown in Figure 3b for FL-MoS_2. How to reveal and use them is a challenge for future experiments. Two-dimensional crystals and other materials could be "combined" to form various hybrids and heterostructures, creating "materials on demand"[53] with properties tailored for targeted applications. In such structures, layer coupling, strain, charge transfer, lattice variations, and interface diffusion will change the band structure, Fermi level, and band offsets. Raman scattering as a nondestructive measurement at room temperature under ambient pressure is ideal to probe the variations of properties from those of the constituent materials. Indeed, Raman scattering was applied in twisted BLG to reveal changes in band structure, with appearance of angle-dependent van Hove singularities.[62]

Conflict of Interest: The authors declare no competing financial interest.

Acknowledgment. We acknowledge M. Bruna for useful discussions, and funding from ERC Grant NANOPOTS, EU Grants RODIN, MEM4WIN, and CareRAMM, EPSRC Grants EP/K01711X/1, EP/K017144/1, and EP/G042357/1, a Royal Society Wolfson Research Merit Award, Nokia Research Centre Cambridge, the Newton Trust and the Newton International Fellowship, the special funds for Major State Basic Research of China (Contract No. 2009CB929301), and the National Natural Science Foundation of China (Grants 11225421 and 10934007).

REFERENCES AND NOTES

1. Geim, A. K.; Novoselov, K. S. The Rise of Graphene. *Nat. Mater.* **2007**, *6*, 183–191.
2. Radushkevich, L. V; Lukyanovich, V. M. O. Strukture Ugleroda, Obrazujucegosja Pri ter-Miceskom Razlozenii Okisi Ugleroda na Zeleznom Kontakte. *Z. Fis. Chim.* **1952**, *26*, 88–95.
3. Oberlin, A.; Endo, M.; Koyama, T. Filamentous Growth of Carbon through Benzene Decomposition. *J. Cryst. Growth* **1976**, *32*, 335–349.
4. Iijima, S. Helical Microtubules of Graphitic Carbon. *Nature* **1991**, *354*, 56–58.
5. Iijima, S.; Ichihashi, T. Single-Shell Carbon Nanotubes of 1-nm Diameter. *Nature* **1993**, *363*, 603–605.
6. Dresselhaus, M. S.; Dresselhaus, G.; Avouris, P. *Carbon Nanotubes: Synthesis, Structure, Properties, and Applications Topics in Applied Physics*; Springer: New York, 2001; Vol. 80.
7. Rao, C. N. R.; Voggu, R.; Govindaraj, A. Selective Generation of Single-Walled Carbon Nanotubes with Metallic, Semiconducting and Other Unique Electronic Properties. *Nanoscale* **2009**, *1*, 96–105.
8. Hersam, M. C. Progress towards Monodisperse Single-Walled Carbon Nanotubes. *Nat. Nanotechnol.* **2008**, *3*, 387–394.
9. Bonaccorso, F.; Hasan, T.; Tan, P. H.; Sciascia, C.; Privitera, G.; Di Marco, G.; Gucciardi, P. G.; Ferrari, A. C. Density Gradient Ultracentifugation of Nanotubes: Interplay of Bundling and Surfactant Encapsulation. *J. Phys. Chem. C* **2010**, *114*, 17267–17285.
10. Shen, C.; Brozena, A. H.; Wang, Y. Double-Walled Carbon Nanotubes: Challenges and Opportunities. *Nanoscale* **2011**, *3*, 503–518.
11. Liang, S. D. Intrinsic Properties of Electronic Structure in Commensurate Double-Wall Carbon Nanotubes. *Phys. B* **2004**, *352*, 305–311.
12. Wang, F.; Sfeir, M. Y.; Huang, L. M.; Huang, X. M. H.; Wu, Y.; Kim, J.; Hone, J.; O'Brien, S.; Brus, L. E.; Heinz, T. F. Interactions between Individual Carbon Nanotubes Studied by Rayleigh Scattering Spectroscopy. *Phys. Rev. Lett.* **2006**, *96*, 167401.
13. Walsh, A. G.; Vamivakas, A. N.; Yin, Y.; Cronin, S. B.; Unlu, M. S.; Goldberg, B. B.; Swan, A. K. Screening of Excitons in Single, Suspended Carbon Nanotubes. *Nano Lett.* **2007**, *7*, 1485–1488.
14. Tan, P. H.; Rozhin, A. G.; Hasan, T.; Hu, P.; Scardaci, V.; Milne, W. I.; Ferrari, A. C. Photoluminescence Spectroscopy of Carbon Nanotube Bundles: Evidence for Exciton Energy Transfer. *Phys. Rev. Lett.* **2007**, *99*, 137402.
15. Ferrari, A. C.; Robertson, J. Raman Spectroscopy in Carbons: From Nanotubes to Diamond. *Philos. Trans. R. Soc., A* **2004**, *362*, 2269–2565.
16. Fantini, C.; Jorio, A.; Souza, M.; Strano, M. S.; Dresselhaus, M. S.; Pimenta, M. A. Optical Transition Energies for Carbon Nanotubes from Resonant Raman Spectroscopy: Environment and Temperature Effects. *Phys. Rev. Lett.* **2004**, *93*, 147406.
17. Piscanec, S.; Lazzeri, M.; Robertson, J.; Ferrari, A. C.; Mauri, F. Optical Phonons in Carbon Nanotubes: Kohn Anomalies, Peierls Distortions,

and Dynamic Effects. *Phys. Rev. B* **2007**, *75*, 035427.
18. Hirschmann, T. Ch.; Araujo, P. T.; Muramatsu, H.; Zhang, X.; Nielsch, K.; Kim, Y. A.; Dresselhaus, M. S. Characterization of Bundled and Individual Triple-Walled Carbon Nanotubes by Resonant Raman Spectroscopy. *ACS Nano* **2013**, 10.1021/nn3055708.
19. Neugebauer, P.; Orlita, M.; Faugeras, C.; Barra, A.-L.; Potemski, M. How Perfect Can Graphene Be? *Phys. Rev. Lett.* **2009**, *103*, 136403.
20. Elias, D. C.; Gorbachev, R. V.; Mayorov, A. S.; Morozov, S. V.; Zhukov, A. A.; Blake, P.; Ponomarenko, L. A.; Grigorieva, I. V.; Novoselov, K. S.; Guinea, F.; *et al.* Dirac Cones Reshaped by Interaction Effects in Suspended Graphene. *Nat. Phys.* **2011**, *7*, 701–704.
21. Ni, Z. H.; Ponomarenko, L. A.; Nair, R. R.; Yang, R.; Anissimova, S.; Grigorieva, I. V.; Schedin, F.; Blake, P.; Shen, Z. X.; Hill, E. H.; *et al.* On Resonant Scatterers as a Factor Limiting Carrier Mobility in Graphene. *Nano Lett.* **2010**, *10*, 3868–3872.
22. Mayorov, A. S.; Gorbachev, R. V.; Morozov, S. V.; Britnell, L.; Jalil, R.; Ponomarenko, L. A.; Blake, P.; Novoselov, K. S.; Watanabe, K.; Taniguchi, T.; *et al.* Micrometer-Scale Ballistic Transport in Encapsulated Graphene at Room Temperature. *Nano Lett.* **2011**, *11*, 2396–2399.
23. Mak, K. F.; Lee, C.; Hone, J.; Shan, J.; Heinz, T. F. Atomically Thin MoS_2: A New Direct-Gap Semiconductor. *Phys. Rev. Lett.* **2010**, *105*, 136805.
24. Latil, S.; Meunier, V.; Henrard, L. Massless Fermions in Multilayer Graphitic Systems with Misoriented Layers: *Ab Initio* Calculations and Experimental Fingerprints. *Phys. Rev. B* **2007**, *76*, 201402(R).
25. Zhang, Y.; Tang, T.-T.; Girit, C.; Hao, Z.; Martin, M. C.; Zettl, A.; Crommie, M. F.; Shen, Y. R.; Wang, F. Direct Observation of a Widely Tunable Bandgap in Bilayer Graphene. *Nature* **2009**, *459*, 820–823.
26. Craciun, M. F.; Russo, S.; Yamamoto, M.; Oostinga, J. B.; Morpurgo, A. F.; Tarucha, S. Trilayer Graphene Is a Semimetal with a Gate-Tunable Band Overlap. *Nat. Nanotechnol.* **2009**, *4*, 383–388.
27. Lui, C. H.; Li, Z.; Mak, K. F.; Cappelluti, E.; Heinz, T. F. Observation of an Electrically Tunable Band Gap in Trilayer Graphene. *Nat. Phys.* **2011**, *7*, 944–947.
28. Ferrari, A. C.; Robertson, J. Interpretation of Raman Spectra of Disordered and Amorphous Carbon. *Phys. Rev. B* **2000**, *61*, 14095–14107.
29. Ferrari, A. C. Raman Spectroscopy of Graphene and Graphite: Disorder, Electron–Phonon Coupling, Doping and Nonadiabatic Effects. *Solid State Commun.* **2007**, *143*, 47–57.
30. Ferrari, A. C.; Meyer, J. C.; Scardaci, V.; Casiraghi, C.; Lazzeri, M.; Mauri, F.; Piscanec, S.; Jiang, D.; Novoselov, K. S.; Roth, S.; *et al.* Raman Spectrum of Graphene and Graphene Layers. *Phys. Rev. Lett.* **2006**, *97*, 187401.
31. Nemanich, R. J.; Lucovsky, G.; Solin, S. A. Long Wavelength Lattice Vibrations of Graphite. In *Proceedings of the International Conference on Lattice Dynamics*; Balkanski, M., Ed.; Flammarion: Paris, France, 1977; pp 619–622.
32. Tan, P. H.; Han, W. P.; Zhao, W. J.; Wu, Z. H.; Chang, K.; Wang, H.; Wang, Y. F.; Bonini, N.; Marzari, N.; Pugno, N.; *et al.* The Shear Mode of Multilayer Graphene. *Nat. Mater.* **2012**, *11*, 294–300.
33. Lui, C. H.; Heinz, T. F. Layer Breathing Modes in Few-Layer Graphene. **2012**, DOI: arXiv:1210.0960v1.
34. Verble, J. L.; Wieting, T. J. Lattice Mode Degeneracy in MoS_2 and Other Layer Com-pounds. *Phys. Rev. Lett.* **1970**, *25*, 362.
35. Eklund, P. C.; Holden, J. M.; Jishi, R. A. Vibrational Modes of Carbon Nanotubes: Spectroscopy and Theory. *Carbon* **1995**, *33*, 959–972.
36. Telg, H.; Maultzsch, J.; Reich, S.; Hennrich, F.; Thomsen, C. Chirality Distribution and Transition Energies of Carbon Nanotubes. *Phys. Rev. Lett.* **2004**, *93*, 177401.
37. Wilson, J. A.; Yoffe, A. D. The Transition Metal Dichalcogenides Discussion and Interpretation of the Observed Optical, Electrical and Structural Properties. *Adv. Phys.* **1969**, *18*, 193–335.
38. Qi, X.-L.; Zhang, S.-C. Topological Insulators and Superconductors. *Rev. Mod. Phys.* **2011**, *83*, 1057–1110.
39. Bonaccorso, F.; Lombardo, A.; Hasan, T.; Sun, Z.; Colombo, L.; Ferrari, A. C. Production and Processing of Graphene and 2D Crystals. *Mater. Today* **2012**, *15*, 564–589.
40. Prasad, S. V.; Zabinski, J. S. Lubricants: Super Slippery Solids. *Nature* **1997**, *387*, 761–763.
41. Khan, U.; May, P.; O'Neill, A.; Bell, A. P.; Boussac, E.; Martin, A.; Semple, J.; Coleman, J. N. Polymer Reinforcement Using Liquid-Exfoliated Boron Nitride Nanosheets. *Nanoscale* **2013**, *5*, 581–587.
42. Mishra, S. K.; Satpathy, S.; Jepsen, O. Electronic Structure and Thermoelectric Properties of Bismuth Telluride and Bismuth Selenide. *J. Phys.: Condens. Matter* **1997**, *9*, 461.
43. Poizot, P.; Laruelle, S.; Grugeon, S.; Dupont, L.; Tarascon, J.-M. Nano-Sized Transition-Metal Oxides as Negative-Electrode Materials for Lithium-Ion Batteries. *Nature* **2000**, *407*, 496–499.
44. Abruna, H. D.; Bard, A. J. Semiconductor Electrodes. 44. Photoelectrochemistry at Polycrystalline p-Type WSe_2 Films. *J. Electrochem. Soc.* **1982**, *129*, 673–675.
45. Djemal, G.; Müller, N.; Lachish, U.; Cahen, D. Photoelectrochemical Cells Using Polycrystalline and Thin Film MoS_2 Electrodes. *Sol. Energy Mater. Sol. Cells* **1981**, *5*, 403–416.
46. Frey, G. L.; Reynolds, K. J.; Friend, R. H.; Cohen, H.; Feldman, Y. Solution-Processed Anodes from Layer-Structure Materials for High-Efficiency Polymer Light-Emitting Diodes. *J. Am. Chem. Soc.* **2003**, *125*, 5998–6007.
47. Clement, R. P.; Davies, W. B.; Ford, K. A.; Green, M. L. H.; Jacobson, A. J. Organometallic Intercalates of the Layered Transition-Metal Dichalcogenides Tantalum Sulfide (TaS_2) and Zirconium Sulfide. *Inorg. Chem.* **1978**, *17*, 2754–2758.
48. Kudo, A.; Omori, K.; Kato, H. A Novel Aqueous Process for Preparation of Crystal from Controlled and Highly Crystalline $BiVO_4$ Powder from Layered Vanadates at Room Temperature and Its Photocatalytic and Photophysical Properties. *J. Am. Chem. Soc.* **1999**, *121*, 11459–11467.
49. *Gmelin Handbook of Inorganic and Organometallic Chemistry*, 8th ed.; Springer-Verlag: Berlin, 1995; Vol. B7.
50. Sundaram, R.; Engel, M.; Lombardo, A.; Krupke, R.; Ferrari, A. C.; Avouris, Ph.; Steiner, M. Electroluminescence in Single Layer MoS_2. **2012**, DOI: arXiv:1211.4311.
51. Zhang, X.; Han, W. P.; Wu, J. B.; Milana, S.; Lu, Y.; Li, Q. Q.; Ferrari, A. C.; Tan, P. H. Shear and Layer Breathing Modes in Multilayer MoS_2. *Phys. Rev. B* **2013**, arXiv:1212.6796v1.
52. Lee, C.; Yan, H.; Brus, L. E.; Heinz, T. F.; Hone, J.; Ryu, S. Anomalous Lattice Vibrations of Single- and Few-Layer MoS_2. *ACS Nano* **2010**, *4*, 2695–2700.
53. Novoselov, K. S.; Castro Neto, A. H. Two-Dimensional Crystals-Based Heterostructures: Materials with Tailored Properties. *Phys. Scr.* **2012**, *T146*, 014006.
54. Georgiou, T., Jalil, R.; Belle, B. D.; Britnell, L.; Gorbachev, R. V.; Morozov, S. V.; Kim, Y.-J.; Gholinia, A.; Haigh, S. J.; Makarovsky, O.; *et al.* Vertical Field Effect Transistor based on Graphene-WS2 Heterostructures for Flexible and Transparent Electronics. **2012**, DOI: arXiv:1211.5090.
55. Kroemer, H. A Proposed Class of Heterojunction Injection Lasers. *Proc. IEEE* **1963**, *51*, 1782.
56. Mimura, T.; Hiyamizu, S.; Fujii, T.; Nambu, K. A New Field-Effect Transistor with Selectively Doped GaAs/n-Al_xGa_{1-x} as Heterojunctions. *Jpn. J. Appl. Phys.* **1980**, *19*, L225–L227.
57. Echtermeyer, T. J.; Britnell, L.; Jasnos, P. K.; Lombardo, A.; Gorbachev, R. V.; Grigorenko, A. N.; Geim, A. K.; Ferrari, A. C.; Novoselov, K. S. Strong Plasmonic Enhancement of Photovoltage in Graphene. *Nat. Commun.* **2011**, *2*, 458.
58. Konstantatos, G.; Badioli, M.; Gaudreau, L.; Osmond, J.; Bernechea, M.; De Arquer, F. P. G.; Gatti, F.; Koppens, F. H. L. Hybrid Graphene-Quantum Dot Phototransistors with Ultrahigh Gain. *Nat. Nanotechnol.* **2012**, *7*, 363–368.

59. Zhao, W. J.; Tan, P. H.; Liu, J.; Ferrari, A. C. Intercalation of Few-Layer Graphite Flakes with $FeCl_3$: Raman Determination of Fermi Level, Layer by Layer Decoupling, and Stability. *J. Am. Chem. Soc.* **2011**, *133*, 5941–5946.
60. Schedin, F.; Lidorikis, E.; Lombardo, A.; Kravets, V. G.; Geim, A. K.; Grigorenko, A. N.; Novoselov, K. S.; Ferrari, A. C. Surface Enhanced Raman Spectroscopy of Graphene. *ACS Nano* **2010**, *4*, 5617–5626.
61. Dang, W. H.; Peng, H. L.; Li, H.; Wang, P.; Liu, Z. F. Epitaxial Heterostructures of Ultrathin Topological Insulator Nanoplate and Graphene. *Nano Lett.* **2010**, *10*, 2870–2876.
62. Kim, K.; Coh, S.; Tan, L. Z.; Regan, W.; Yuk, J. M.; Chatterjee, E.; Crommie, M. F.; Cohen, M. L.; Louie, S. G.; Zettl, A. Raman Spectroscopy Study of Rotated Double-Layer Graphene: Misorientation-Angle Dependence of Electronic Structure. *Phys. Rev. Lett.* **2012**, *108*, 256103.